BEST AVAILABLE IMAGES

Defective images within this document are accurate representations of the original documents submitted by the applicant.

Defects in the images may include (but are not limited to):

- BLACK BORDERS
- TEXT CUT OFF AT TOP, BOTTOM OR SIDES
- FADED TEXT
- ILLEGIBLE TEXT
- SKEWED/SLANTED IMAGES
- COLORED PHOTOS
- BLACK OR VERY BLACK AND WHITE DARK PHOTOS
- GRAY SCALE DOCUMENTS

IMAGES ARE BEST AVAILABLE COPY.

As rescanning documents *will not* correct images, please do not report the images to the Image Problem Mailbox.

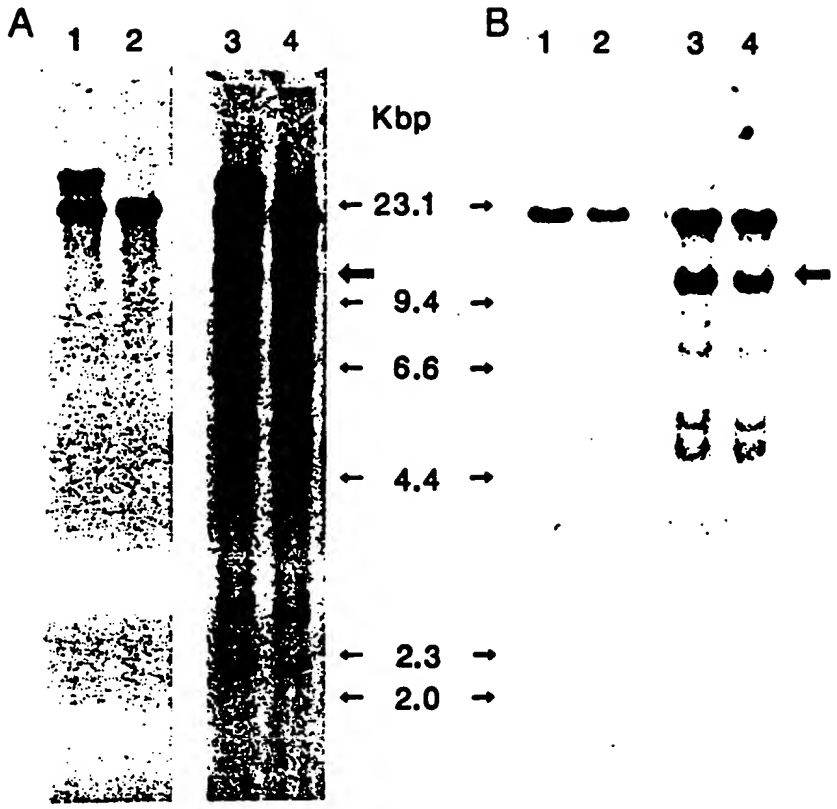

Figure 1. Detection of v-*fms* and PDGF receptor-related gene fragments in human placenta and thymus DNAs. Hybridization of a v-*fms* probe (A) or a mouse PDGF receptor probe (B) to human placenta (lane 1 and 3) or thymus (lane 2 and 4) DNAs under stringent (50% formamide; lane 1 and 2) or relaxed (30% formamide; lane 3 and 4) hybridization conditions. Arrows indicate the 12-kbp *Eco*RI fragment detected under relaxed conditions by both v-*fms* and mouse PDGF-R probes.

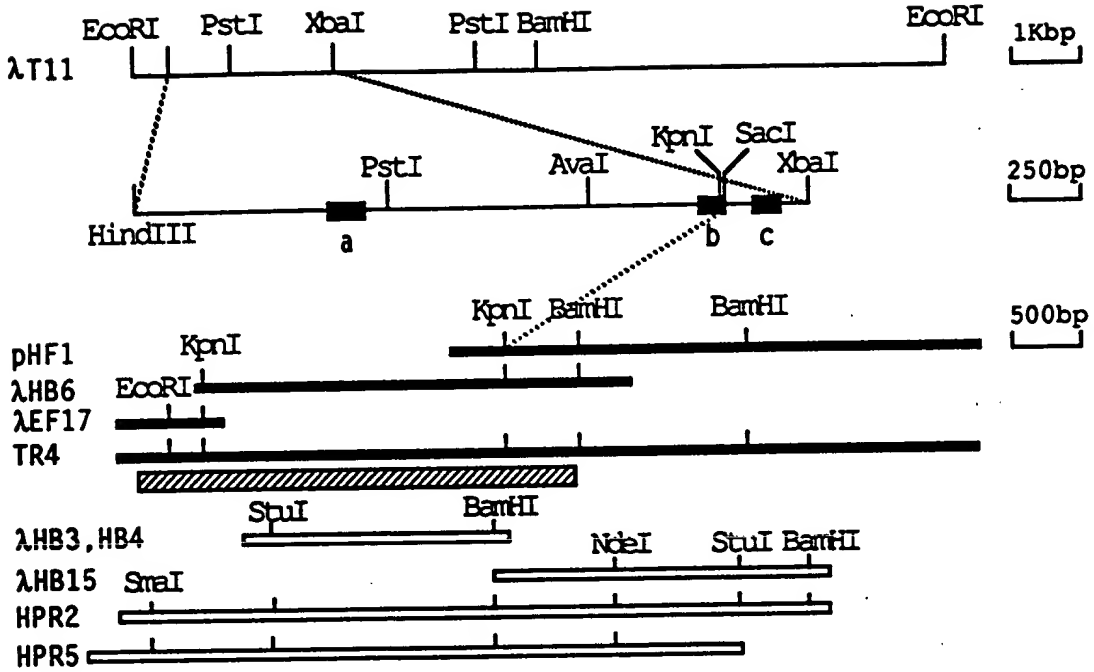

Figure 2. Molecular cloning of the λT11 genomic fragment as well as cDNAs of T11 and PDGF-R genes. Restriction map of: λT11 genomic clone (solid lines); T11 cDNA clones (solid bars); and PDGF-R cDNA clones (open bars). Coding regions within three fragments, as determined by nucleotide sequencing analysis, are indicated by black boxes labeled a, b and c.

Figure 3. See Legend on next page

Figure 3. T11 cDNA nucleotide and predicted amino acid sequences. Nucleotides are numbered at the left. The predicted amino acid sequence of the long open reading frame is shown above the nucleotide sequence. Amino acids are numbered over the amino acids, starting at the putative initiation codon. The potential N-terminal signal sequence is underlined. Potential sites of N-linked glycosylation are overlined, and cysteine residues are boxed. The putative single transmembrane region is indicated by a shaded bar. The potential ATP binding site in the kinase domain is indicated by circles over Gly at residues 600, 602 and 605 and Lys at residue 627. The putative tyrosine autophosphorylation site at residue 849 is indicated by *. The regions of the λT11 genomic sequence defined by exons a, b and c are underlined. The AATAAA box close to the polyadenylated 3' end of the cDNA is underlined as well.

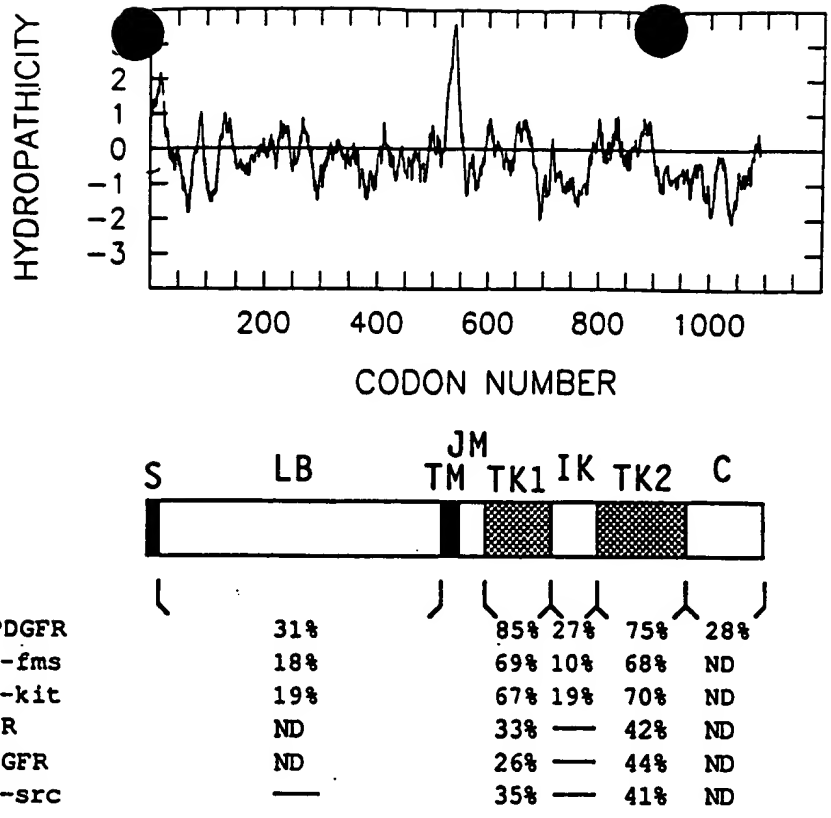

Figure 4. Hydropathicity profile and homology with other tyrosine kinases of the T11 receptor-like gene product. A schematic diagram of the predicted protein domains shows the signal sequence (S; black box), ligand binding domain (LB), transmembrane domain (TM; second black box), juxtamembrane domain (JM), tyrosine kinase domains (TK1, TK2; hatched boxes), inter-kinase domain (IK) and carboxyl terminus (C). The hydropathicity profile was calculated by the method of Kyte and Doolittle (46). The homology percentages shown refer to identical amino acids within each respective domain. Abbreviations: IR, insulin receptor; EGF-R, epidermal growth factor receptor; ND, not determined.

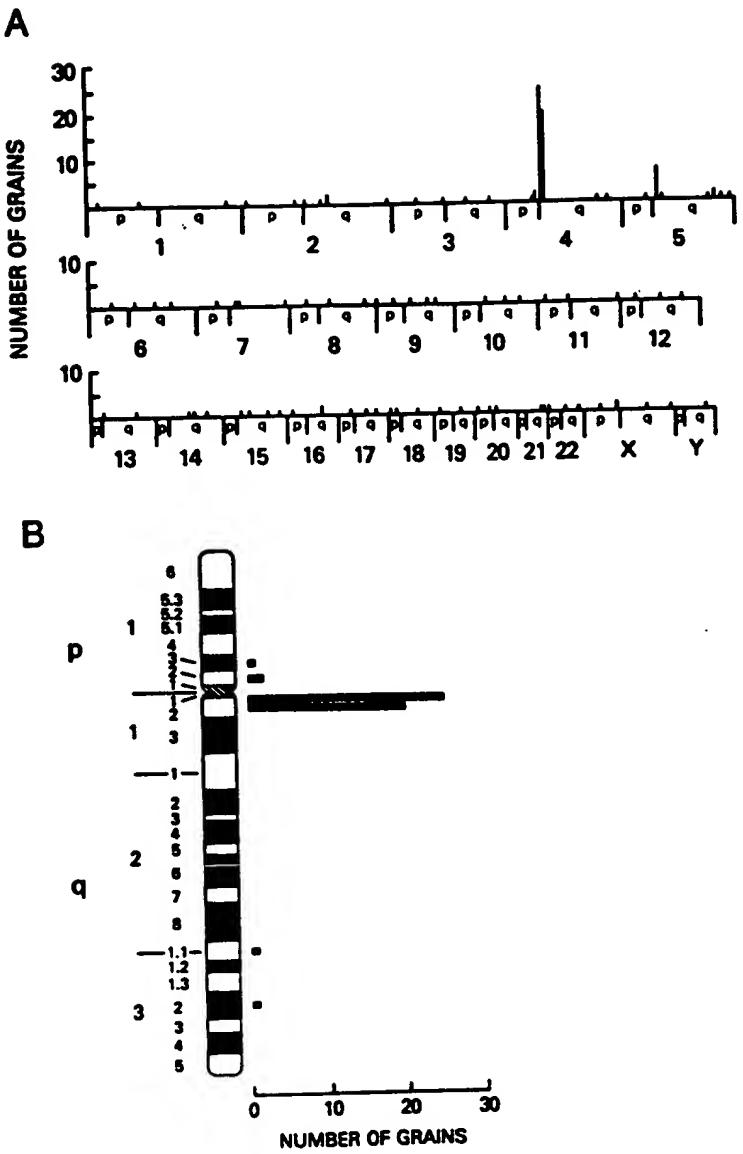

Figure 5. Chromosome mapping of the T11 gene. (A) Distribution of silver grains on normal human chromosomes by *in situ* hybridization with pT11-P probe (clone of the 3.6-kbp *Pst*I genomic fragment) (see Fig. 1). (B) Distribution of grains on chromosome 4.

Figure 6. See Legend on next page.

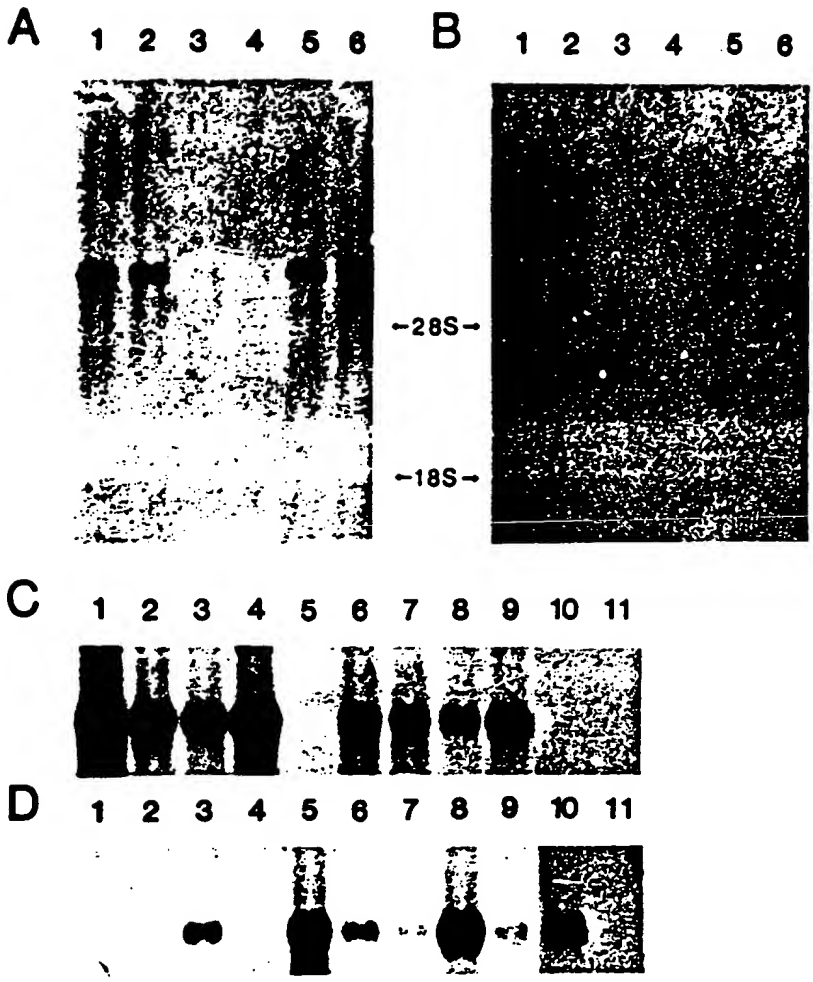

Figure 6. Comparison of mRNA species of the T11 and known PDGF-R genes, in normal and tumor cells. The same filter was first hybridized with the probe from pT11-HP (0.95-kbp *Hind*III-*Pst*I genomic fragment) (A) and then rehybridized with a PDGF-R cDNA probe (B). A different filter was first hybridized with T11 cDNA (3.5-kbp *Bam*HI fragment of TR4 including the whole coding region) (C) and then rehybridized with PDGF-R cDNA (3.8-kbp *Nde*I fragment of HPR2) (D). A and B contained poly (A)+ RNAs (5 μg per lane) extracted from human smooth muscle (lane 1), heart (lane 2), liver (lane 3), spleen (lane 4) or embryo (lanes 5 and 6). C and D contained total RNA (20 μg per lane) extracted from G402 leiomyoblastoma cells (lane 1), SK-LMS-1 leiomyosarcoma cells (lane 2), A1186 or A204 rhabdomyosarcoma cells (lanes 3 and 4), 8387 fibrosarcoma cells (lane 5), astrocytoma tissues (lanes 6 and 7), A1690 astrocytoma cells (lane 8), A1207 or A172 glioblastoma cells (lanes 9 and 10) or A875 melanoma cells (lane 11). Migrations of 28S and 18S ribosomal RNA (markers) are as indicated.

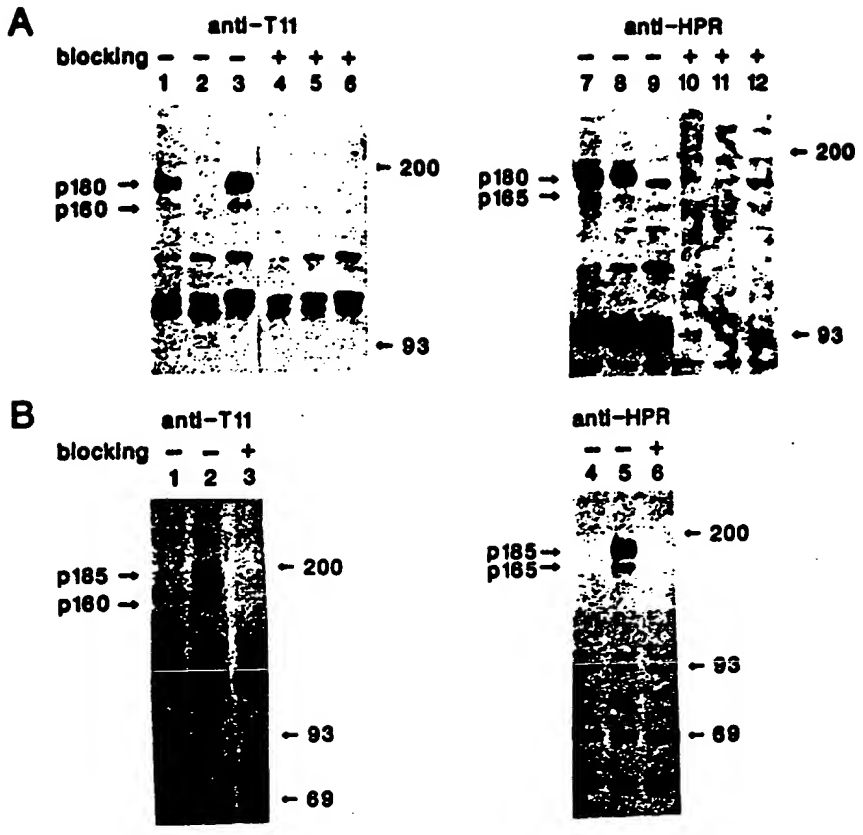

Figure 7. Detection of T11 and PDGF-R proteins with peptide antisera in human cell lines (A) and COS-1 cell transfectants (B). (A) M426 human embryo fibroblasts (lanes 1, 4, 7 and 10), 8387 fibrosarcoma cells (lanes 2, 5, 8 and 11), A204 rhabdomyosarcoma cells (lanes 3, 6, 9 and 12), (B) COS-1 cells (lanes 1 and 4), COS-1 cells transfected with vectors carrying T11 cDNA (lanes 2 and 3) or PDGF-R cDNA (lanes 5 and 6).

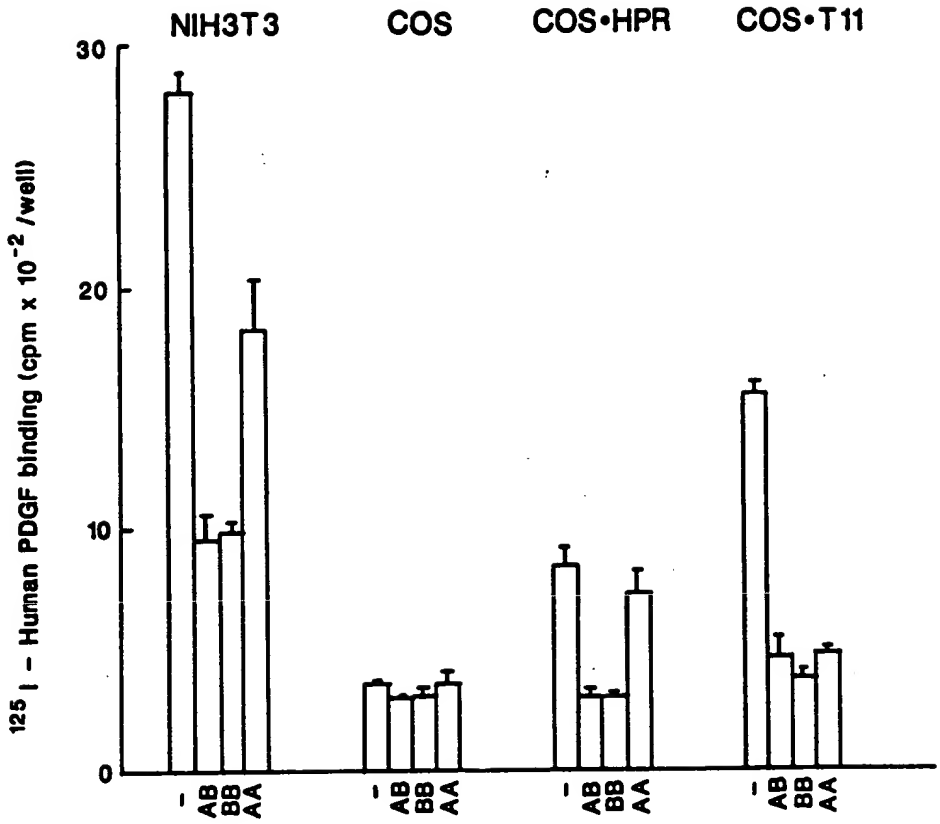

Figure 8. Binding of ^{125}I-labeled human PDGF to mouse control NIH/3T3, control COS-1 and COS-1 cells transfected with T11 or known PDGF-R cDNA expression vectors. Results represent the mean values (±SD), of triplicate samples.

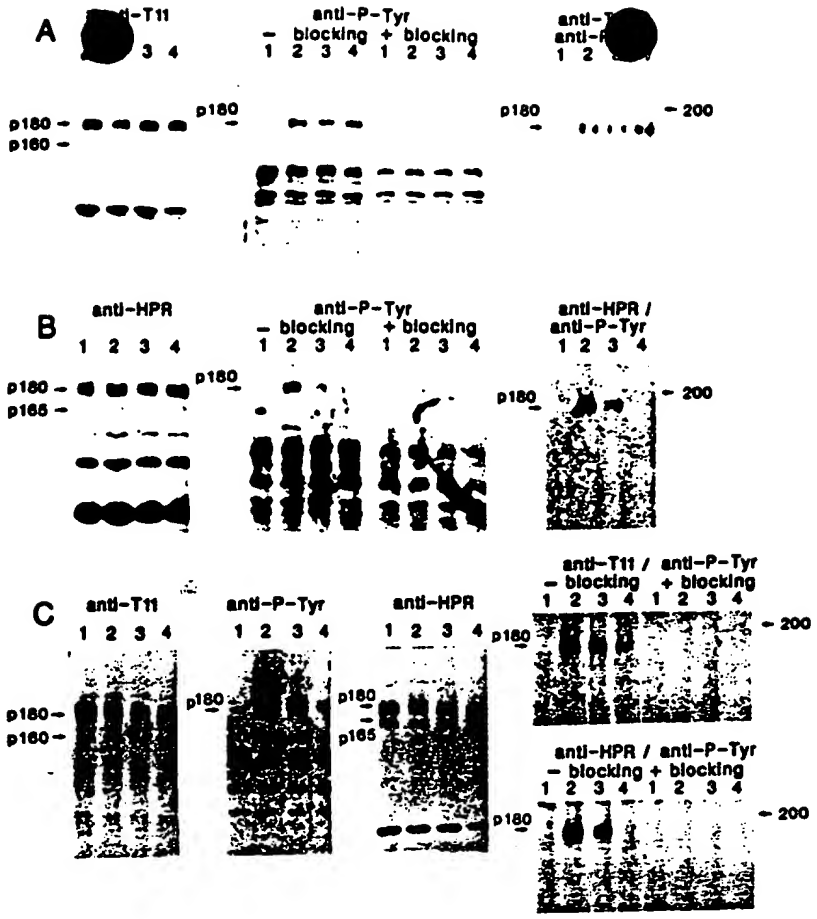

Figure 9. Tyrosine autophosphorylation of type α and type β PDGF-R gene products induced by different PDGF isoforms. A204 (A), 8387 (B), or NIH/3T3 (C) cells were incubated with PDGF-BB (30 ng/ml) (lane 2), human PDGF (30 ng/ml) (lane 3), PDGF-AA (300 ng/ml) (lane 4) or 3 mM acetic acid (vehicle control: lane 1). Cell lysates were immunoprecipitated with peptide antisera directed against predicted type α or type β PDGF receptors (anti-T11 and anti-HPR, respectively). Immunoblot analyses was with antibodies to the receptors or phosphotyrosine (anti-P-Tyr) (54) as indicated above the blots. Arrows indicate the specific bands which were blocked in the presence of immunizing peptide.

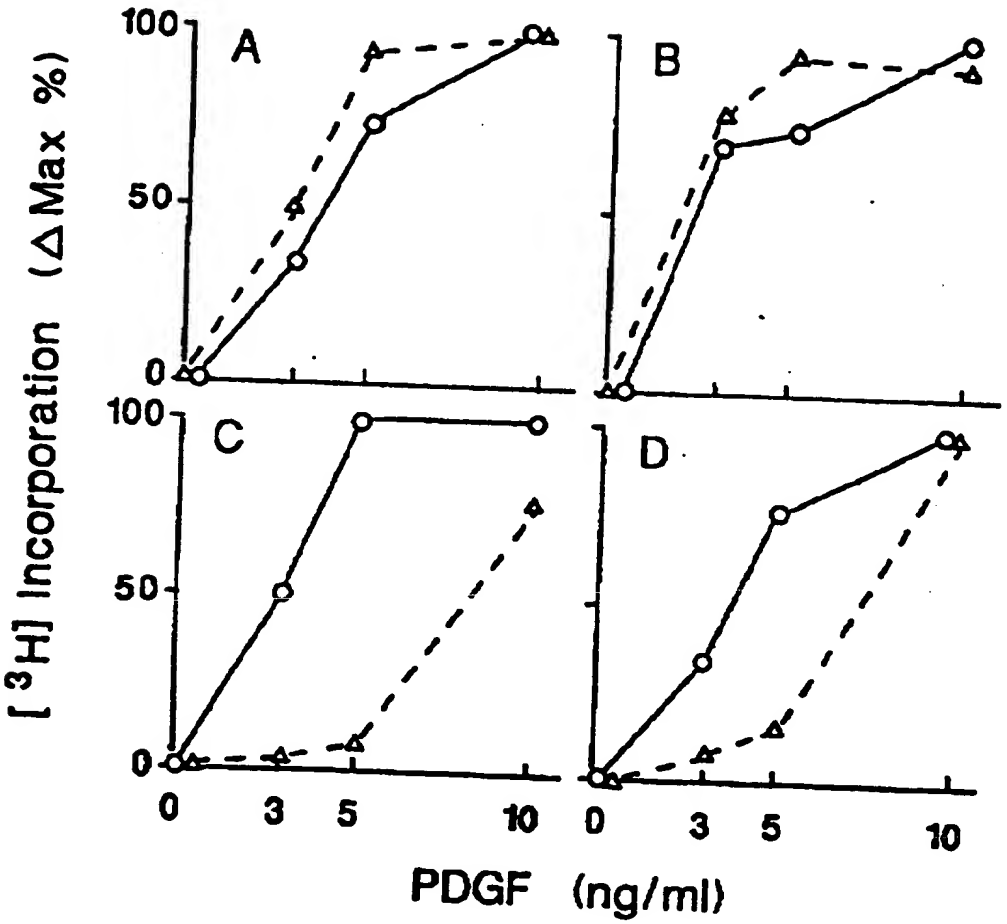

Figure 10. Stimulation of DNA synthesis by PDGF-AB (triangles) or PDGF-BB (circles) in various cells, as follows: (A) mouse NIH/3T3; (B) human M426; (C) human AG1523; (D) human M413.

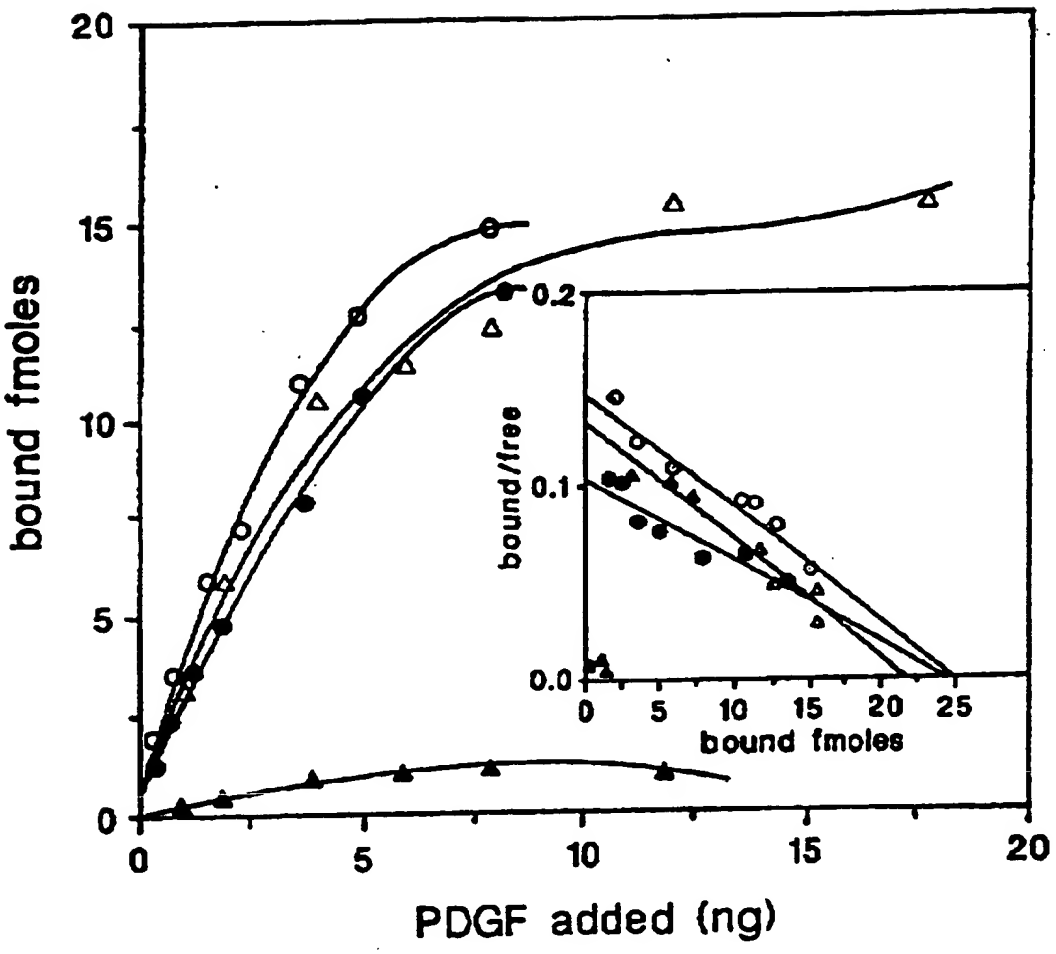

Figure 11. Receptor binding of PDGF-AB (triangles) or PDGF-BB (circles) by human D32 cells reconstituted with type α (open symbols) or type β (filled symbols) PDGF receptors by transfection with vectors bearing the respective cDNAs. The inset displays the same data replotted in the standard (semi-log) Scatchard format.

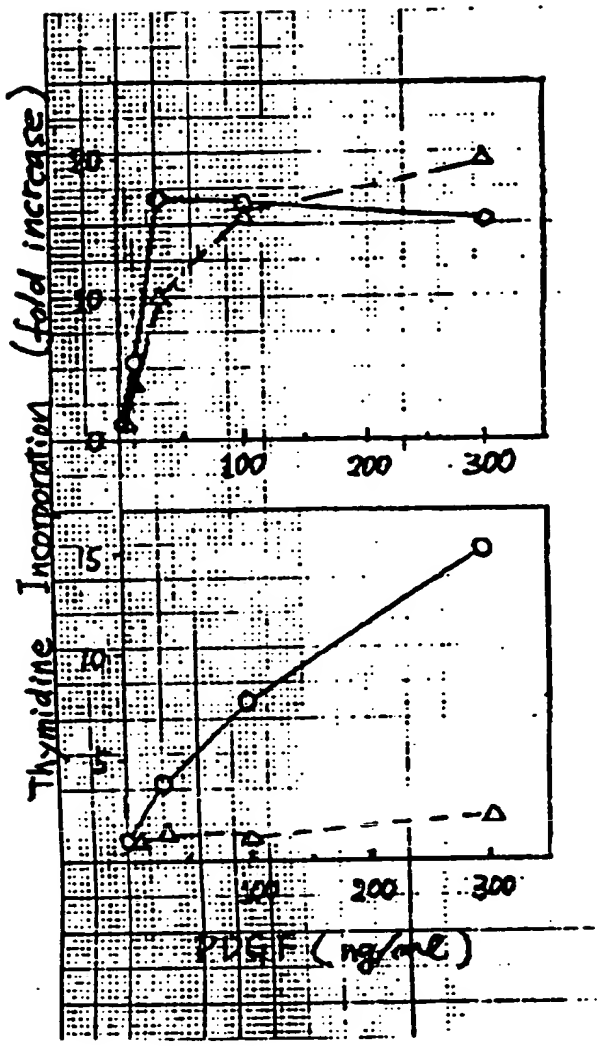

Figure 12. DNA synthesis stimulation responses to PDGF-AB (triangles) or PDGF-BB (circles) by human D32 cells reconstituted with type α (upper panel) or type β (lower panel) PDGF receptors.

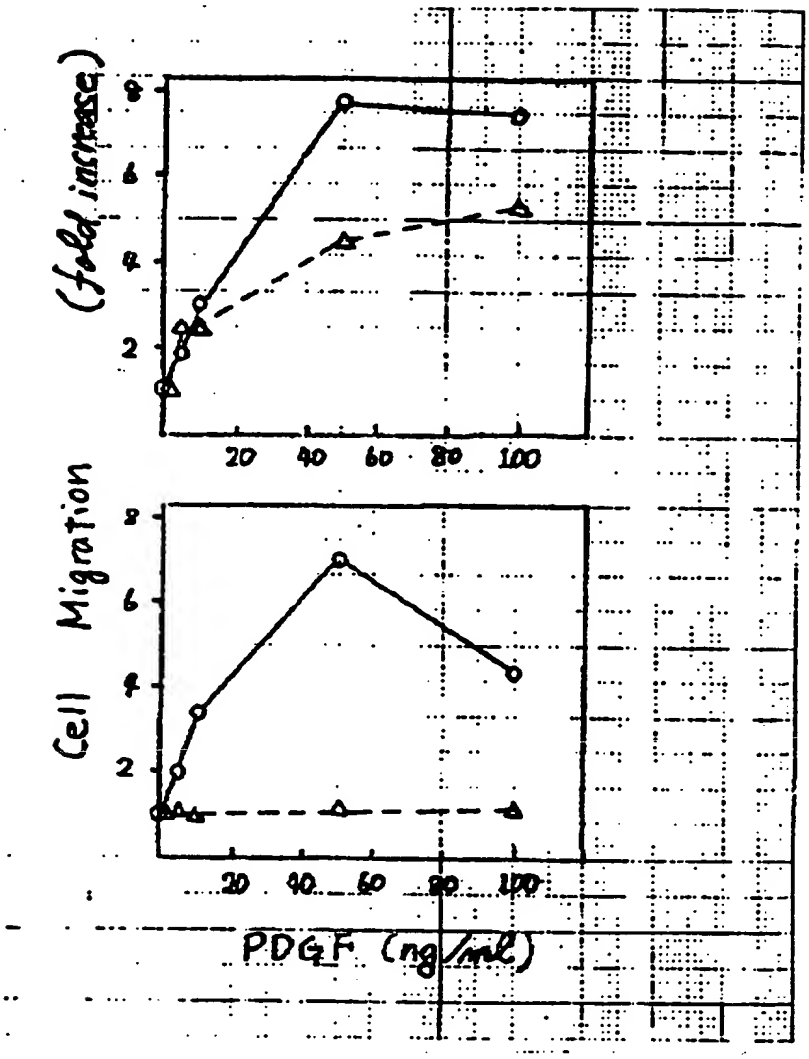

Figure 13. Chemotaxic responses to PDGF-AB (triangles) or PDGF-BB (circles) by human D32 cells reconstituted with type α (upper panel) or type β (lower panel) PDGF receptors.

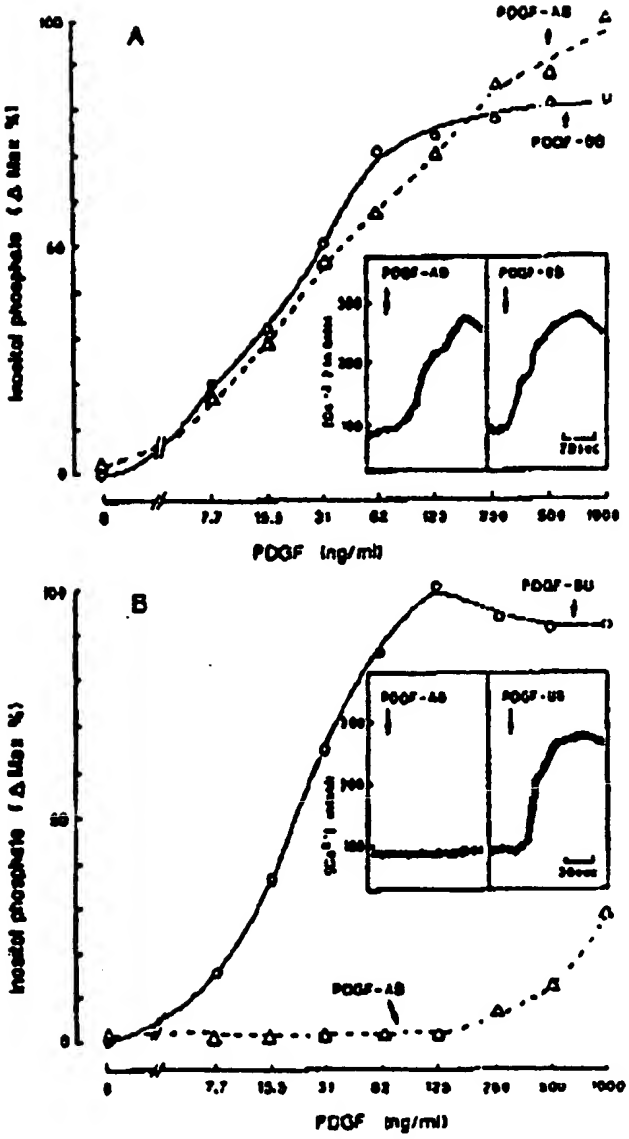

Figure 14. Responses of inositol phosphate formation and cytosolic calcium ion mobilization (i.e., $[Ca^{2+}]i$; data in insets) to PDGF-AB (triangles) or PDGF-BB (circles) by human D32 cells reconstituted with type α (upper panel) or type β (lower panel) PDGF receptors.